

Two dimensional electron gas in the δ -doped iridates with strong spin-orbit coupling: $\text{La}_\delta\text{Sr}_2\text{IrO}_4$

Churna Bhandari and S. Satpathy

Department of Physics & Astronomy, University of Columbia Missouri, Columbia, MO 65211

(Dated: February 5, 2019)

Iridates are of considerable current interest because of the strong spin-orbit coupling that leads to a variety of new phenomena. Using density-functional studies, we predict the formation of a spin-orbital entangled two dimensional electron gas (2DEG) in the δ -doped iridate $\text{La}_\delta\text{Sr}_2\text{IrO}_4$, where a single SrO layer is replaced by a LaO layer. The extra La electron resides close to the δ -doped layer, partially occupying the $J_{\text{eff}} = 1/2$ upper Hubbard band and thereby making the interface metallic. The magnetic structure of the bulk is destroyed near the interface, with the Ir_0 layer closest to the interface becoming non-magnetic, while the next layer (Ir_1) continues to maintain the AFM structure of the bulk, but with a reduced magnetic moment. The Fermi surface consists of a hole pocket and an electron pocket, located in two different Ir layers (Ir_0 and Ir_1), with both carriers derived from the $J_{\text{eff}} = 1/2$ upper Hubbard band. The presence of both electrons and holes at the δ -doped interface suggests unusual transport properties, leading to possible device applications.

The combination of a large spin-orbit coupling (SOC) and a reduced Coulomb interaction in the 4d and 5d transition metal oxides has made these compounds hosts for a number of exotic quantum states, such as the spin-orbit driven Mott insulators¹, Weyl semimetals², axion insulators^{3,4}, and Kitaev spin liquids.^{5,6} Analogously, one expects any two dimensional electron gas (2DEG) formed in the Sr_2IrO_4 (SIO) iridate structures⁷, similar to the 3d interfaces such as $\text{LaAlO}_3/\text{SrTiO}_3$ ⁸, to lead to potentially novel effects due to the spin-orbital entanglement of the electron states. Recently, epitaxial growth of iridate heterostructures and interfaces has been demonstrated by a number of experiments⁹⁻¹¹, which paves the way for the engineering of δ -doped iridates structures by substitution of an element with another having an excess electron or hole. Such δ -doped structures can further lead to the formation of 2DEG near the dopants.

The characteristic electronic properties of the iridates are controlled by the Ir^{4+} ion in the d^5 configuration. A large crystal field splits the d states into two e_g and three t_{2g} states. The sixfold t_{2g} manifold (including spin) is further split into a fourfold $J_{\text{eff}} = 3/2$ and a twofold $J_{\text{eff}} = 1/2$ manifold, with an energy gap of $\lambda_{\text{SOC}} = 3\lambda/2$, $\lambda\vec{L} \cdot \vec{S}$ being the SOC interaction. Four electrons fill the lower-lying $J_{\text{eff}} = 3/2$ states, leaving the lone d electron to occupy the doubly degenerate $J_{\text{eff}} = 1/2$ state. The wave functions $|J_{\text{eff}}, m\rangle$ are spin-orbital entangled, viz.,

$$\begin{aligned} |e_1\rangle &\equiv \left|\frac{1}{2}, -\frac{1}{2}\right\rangle = (|xy \uparrow\rangle + |yz \downarrow\rangle + i|xz \downarrow\rangle)/\sqrt{3}, \\ |e_2\rangle &\equiv \left|\frac{1}{2}, \frac{1}{2}\right\rangle = (|yz \uparrow\rangle - i|xz \uparrow\rangle - |xy \downarrow\rangle)/\sqrt{3}. \end{aligned} \quad (1)$$

The half-filled $J_{\text{eff}} = 1/2$ band splits further due to the Coulomb interaction into an upper Hubbard band (UHB) and a lower Hubbard band (LHB), producing a Mott insulator.

The Mott insulating state can be doped with electrons or holes via impurity substitution. Experimentally, there have been already several studies on the bulk electron doping^{10,12-19} by the substitution of Sr by trivalent metals like La.^{20,21} These bulk doped samples display several interesting features such as the formation of Fermi arcs and pseudogaps by potassium surface doping¹⁷ and a metallic state beyond 5%²² or 15% La.¹⁰

In this paper, we predict the formation of a 2DEG in the δ -doped SIO iridate using density functional methods. The predicted 2DEG is different from a conventional 2DEG obtained at the δ -doped 3d perovskite oxides such as $\text{La}_\delta\text{SrTiO}_3$ structures^{23,24} in several ways, viz., (i) The 2DEG is spin-orbital entangled, (ii) It is sharply localized on just two Ir (Ir_0 and Ir_1) planes adjacent to δ -doped LaO layer as opposed to the $\text{La}_\delta\text{SrTiO}_3$, where it spreads to several unit-cell layers around LaO, and (iii) As opposed to the multi-band Fermi surface for the 3d structures, the Fermi surface is much simpler in the present case, consisting of just one (nearly circular) hole pocket at Γ and an elliptical electron pocket at M point of the 2D interface Brillouin zone.

In our study, we used the full-potential linearized muffin-tin orbital (FP-LMTO) method²⁵⁻²⁷ to solve the density functional Kohn-Sham equations in the local spin density approximation^{28,29} including spin-orbit coupling and the Hubbard U term (LSDA+SOC+U). The supercell consisted of 8 SIO layers stacked along the c -axis and each layer consisted of two formula units, so as to describe the possible anti-ferromagnetic state in each layer, leading to the unit cell consisting of $(\text{Sr}_2\text{IrO}_4)_{16}$. All atom positions were optimized with the lattice constant of the supercell structure fixed at the bulk experimental value. To form the δ -doped structure, we substituted a single layer of SrO by LaO, as indicated in Fig. 1. We also used the Vienna *ab initio* Simulation Package (VASP)³⁰ within the projector augmented wave (PAW)³¹ method including U in the Dubarev scheme³² and SOC for computing magnetic moments. We used the plane wave cut-off energy of 620 eV and a $6 \times 6 \times 1$ \mathbf{k} -mesh for Brillouin zone sampling.

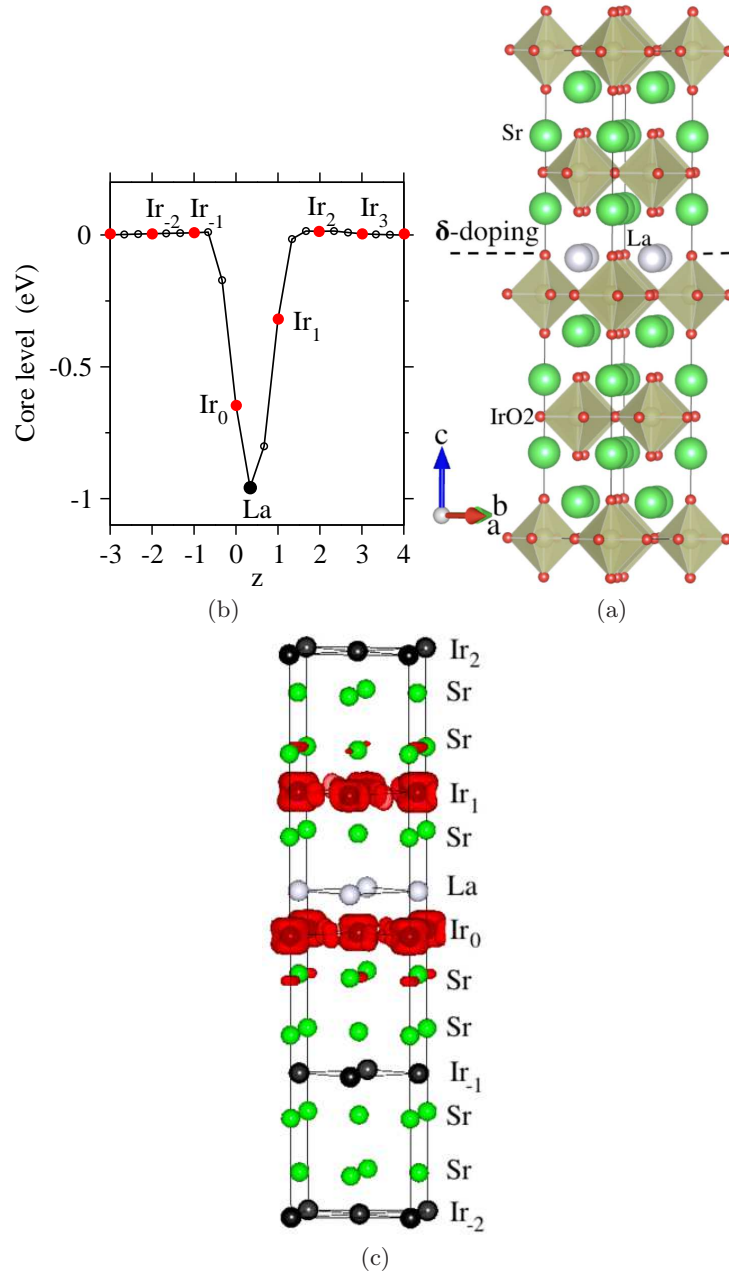


FIG. 1: (a) The δ -doped $\text{La}_5\text{Sr}_2\text{IrO}_4$ structure, with a portion of the supercell shown, (b) The cell averaged O 1s core level energies as a function of the distance from the LaO layer, showing a V-shaped potential, and (c) Charge density contours for the electron bands near E_F , indicating the localization of the 2DEG on the two Ir layers closest to LaO. A small slice of energy (in the range of E_F and $E_F - 0.15$ eV) was used to compute the charge density. The isovalue shown in red corresponds to the charge density of 10^{-3} e/ \AA^3 . Note that in Fig. (a), the Ir atoms occur at the center of the oxygen octahedra.

On general grounds, one expects a V-shaped potential at the δ -doped layer. Since La has an extra valence electron as compared to Sr, with the transfer of these electrons to the solid, the $\text{La}^{+3}\text{O}^{-2}$ layer becomes nominally a positively charged layer as compared to the neutral $\text{Sr}^{+2}\text{O}^{-2}$ layer, and thus it produces a uniform electric field on either side of the infinite 2D plane, leading to a V-shaped attractive potential, in which the extra valence electron of La becomes bound.

The potential due to a charged sheet is simply $V = (\sigma/\epsilon)|z|$, where σ is the surface charge density, ϵ is the dielectric constant, and z is the distance from the interface. The potential near the δ -doped layer may be examined by studying the core level energy shifts. Using density functional theory (DFT), we have computed the O (1s) core energies. The cell averaged core level energies (averaged over the bulk unit cell) are shown in Fig. 1 (b). As one moves away from

TABLE I: Distribution of the δ -doped electron (one per La atom) and the spin and orbital magnetic moments (in units of μ_B) of the Ir atoms in the layers close to the interface. The listed charges are in essence the occupancy n_2 of the UHB belonging to different Ir layers, while the corresponding occupation of the LHB is $n_1 = 1$ for each Ir layer.

atom	Ir ₀	Ir ₁	Ir ₂	Ir ₋₁	rest
charge (e)	0.64	0.18	0	0	0.18
μ_s	0.00	0.06	0.11	0.11	0
μ_l	0.00	0.14	0.28	0.28	0

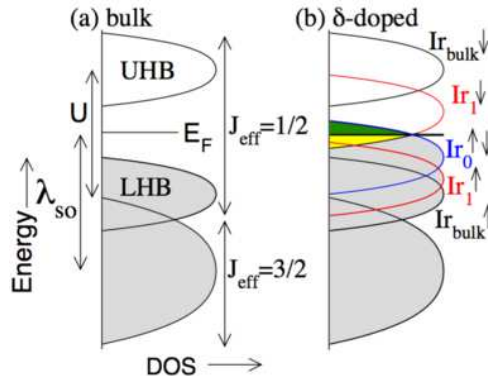


FIG. 2: Schematic electronic structure for the Ir t_{2g} bands for bulk SIO (a) and the δ -doped structure (b), as obtained from the DFT calculations.

the interface, the interfacial potential is screened due to the redistribution of electrons around the donor plane. From the DFT calculations, we find a more or less V -shaped potential close to the interface. Apart from this, Fig. 1 (b) shows that the Ir layers as close as the second layer to LaO (viz., Ir₂ and Ir₋₁) already look like the bulk.

We find that the interface potential is strong enough to localize the δ -doped electrons in the two Ir layers closest to the interface. This may be seen from the charge density of the electron bands near the Fermi energy (E_F). For this purpose, we used the energy range of E_F to 0.15 eV below it. The results shown in Fig. 1 (c) indicate the confinement of the doped electrons to mostly the Ir₀ and Ir₁ layers. The same conclusion is inferred from the computed charges of the individual atoms shown in Table I, which were estimated by computing the total charges within the muffin-tin spheres and renormalizing them to the total number of electrons in the system.

We now turn to the band structure and the Fermi surface. Fig. 2 (a) shows the well known¹ spin-orbit assisted Mott insulating state of the bulk SIO, in terms of which the electron states of the δ -doped structure, shown in Fig. 2 (b), may be understood. The individual Ir layers in the structure are separated enough that the electronic structure can be understood in terms of the isolated layers. The upper and the lower Hubbard bands for the interface Ir layers (Ir₀ and Ir₁) are shifted in energy due to the V -shaped interface potential and, in addition, they show a layer-dependent splitting $2\Delta = U(n_1 - n_2)$ between the LHB and the UHB, with the respective population being n_1 and n_2 . The LHB is full for each Ir layer ($n_1 = 1$), while the UHB is only partially full, $n_2 < 1$ for Ir₀ and Ir₁, and 0 for the remaining Ir atoms, which are similar to the SIO bulk. The charges listed in Table I correspond to the charges n_2 in the UHB for the various layers.

Fig. 3 shows the density functional band structure, computed using the FP-LMTO method and the LSDA+SOC+U functional ($U = 2.7$ eV was used following earlier works on bulk SIO), as well as the model tight-binding (TB) results. The Ir (d) $J_{eff} = 1/2$ bands, split into the UHB and LHB, are the ones that occur around the Fermi energy, and the UHB belonging to different Ir layers can be identified in the band structure as marked in Fig. 3 (a). The layer-projected DOS shown in Fig. 4 indicates the partial occupation of the UHB of the Ir atoms close to the δ -doped layer in order to accommodate the doped electrons, which is consistent with the charge distribution presented in Table I.

To help in the understanding of the band structure, we have considered the Hubbard model on a square lattice with anti-ferromagnetic order as appropriate for a single Ir layer in SIO, keeping the two spin-orbital entangled $J_{eff} = 1/2$ orbitals ($|e_1\rangle$ and $|e_2\rangle$ in Eq. 1). The TB Hubbard Hamiltonian is given by

$$\mathcal{H} = \sum_{\langle ij \rangle \alpha} t_{ij} c_{i\alpha}^\dagger c_{j\alpha} + h.c. + \frac{U}{2} \sum_{i\alpha} n_{i\alpha} n_{i\bar{\alpha}}, \quad (2)$$

where $c_{i\alpha}^\dagger$ creates an electron at site i (which may be sublattice A or B) and orbital $|e_\alpha\rangle$, t_{ij} is the hopping integral,

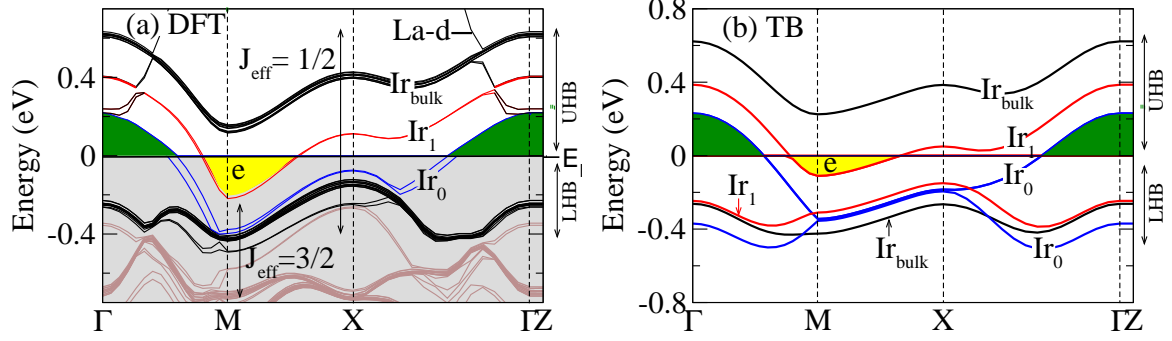


FIG. 3: Band structure of $\text{La}_5\text{Sr}_2\text{IrO}_4$ computed using DFT (a) and the tight-binding model (b). The yellow region represents the electron pocket in the UHB for Ir_1 , while the green region corresponds to the hole pocket in Ir_0 . Both the UHBs and the LHBs originating from various Ir layers are color coded in the TB results, Fig. (b), while in the DFT bands, Fig. (a), only the UHBs can be clearly identified as shown.

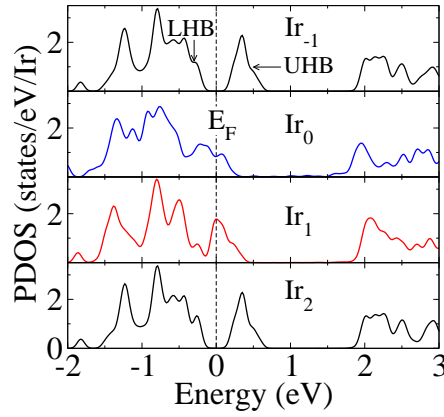


FIG. 4: Layer resolved Ir (d) density of states, indicating the empty UHB in the bulk-like Ir_2 and Ir_{-1} layers, while the same in the Ir_0 and Ir_1 layer are partially filled to accommodate the δ -doped electrons.

U is the on-site Coulomb interaction, and the summation $\langle ij \rangle$ is over distinct pairs of neighbors. The same model parameters, which we used earlier^{7,33} to describe the bulk band structure of SrIrO_3 , were adopted here, viz., $U = 0.65$, $t_1 = -0.095$, $t_2 = 0.015$, $t_3 = 0.035$, and $t_4 = 0.01$, all in units of eV, with t_n being the n -th nearest neighbor hopping.

In the momentum space, the 4×4 Hamiltonian (two sublattice sites in the AFM unit cell and two orbitals per site) becomes block diagonal with two identical 2×2 TB Hamiltonian matrices in the Bloch function basis for $|e_1\rangle$ or $|e_2\rangle$, viz.,

$$\mathcal{H}(\mathbf{k}) = \begin{pmatrix} -\Delta + h_{11}(\mathbf{k}) & h_{12}(\mathbf{k}) \\ h_{12}^*(\mathbf{k}) & \Delta + h_{11}(\mathbf{k}) \end{pmatrix}, \quad (3)$$

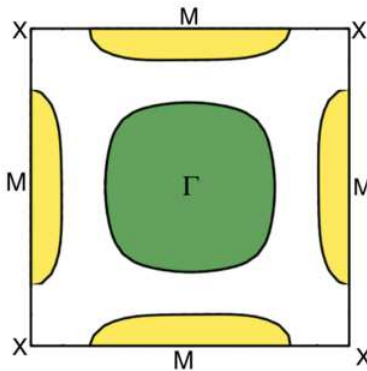


FIG. 5: Fermi surface of the δ -doped structure, consisting of a hole pocket at Γ (green) and an electron pocket at M (yellow).

where $h_{11}(\mathbf{k}) = 4t_2 \cos k_x \cos k_y + 2t_3(\cos 2k_x + \cos 2k_y)$, $h_{12}(\mathbf{k}) = 2t_1(\cos k_x + \cos k_y) + 4t_4(\cos 2k_x \cos k_y + \cos 2k_y \cos k_x)$, the lattice constant of the square lattice is taken as one, and $\Delta = U/2 \times (n_1 - n_2)$ is the Hartree-Fock staggered field with n_α being the occupancy of the $|e_\alpha\rangle$ orbital. One immediately gets the eigenvalues

$$\varepsilon_{\pm}(\mathbf{k}) = h_{11}(\mathbf{k}) \pm \sqrt{\Delta^2 + h_{12}^2(\mathbf{k})}, \quad (4)$$

which are plotted in Fig. 3 (b), where the TB bands for the individual Ir layers are shifted somewhat to fit with the DFT bands.

The bands originating from the various Ir layers are shown in Fig. 3 (b), and the UHBs can be clearly identified in the DFT bands, Fig. 3 (a), as well. Note that the staggered field $\Delta \equiv U(n_1 - n_2)/2$ that characterizes the band splitting between the UHB and the LHB, following Eq. 4, is layer dependent, which leads to different shapes of the bands for different Ir layers, as clearly seen in the TB band structure.

The band structure clearly indicates that the δ -doped electrons occupy the UHB of the Ir₀ and Ir₁ layers. In addition, the layer resolved Ir densities-of-states (DOS) shown in Fig. 4 confirms the same picture. We estimated the amount of δ -doped charge in each layer by integrating the layer projected DOS, which yields 64% for Ir₀, 18% for Ir₁, and the remaining 18% shared among other atoms such as La, O etc. These are the charge density values listed in Table I.

The Fermi surface, shown in Fig. 5, consists of a hole pocket at Γ and an electron pocket at M . An interesting point is that the electrons and holes are spatially separated, with the electron pocket occurring in the Ir₁ layer, while the hole pocket occurs in Ir₀. The presence of both an electron and a hole pocket is quite unusual and it happens because of the presence of multiple bands in the electronic structure, with the nearly empty bands behaving as electrons, while the nearly filled bands behaving like holes. We note that this feature is not always found, e. g., in the La δ -doped perovskite La _{δ} Sr_{1- δ} TiO₃, where also a 2DEG is found along with multiple bands, there is only electron-like behavior.²³ Transport measurements should show the presence of these two different types of carriers, unraveling this unusual behavior.

The 2DEG alters the magnetic moments of the Ir atoms near the δ -doped layer. The computed spin and orbital magnetic moments given in Table I shows that both the spin and orbital magnetic moments, μ_s and μ_l are zero for Ir₀ making it non-magnetic, while for Ir₁, they are roughly half of the bulk values, already achieved in the Ir₂ and the Ir₋₁ layers. For these layers, the calculated net magnetic moment is $0.39 \mu_B$ compared to the calculated $\approx 0.36 \mu_B$ for the bulk.³³ The experimental magnetic moment in the bulk has been estimated to be $0.5 \mu_B$ from magnetic susceptibility measurements.³⁴

In summary, we predicted the formation of a spin-orbital entangled 2DEG in the δ -doped iridate La _{δ} Sr₂IrO₄, where a single layer of SrO is replaced by LaO in the Sr₂IrO₄ crystal. The doped electron remains close to the interface, which becomes metallic, with an electron and a hole pocket forming the Fermi surface, while the bulk, away from the interface is insulating. Experimental observation of the 2DEG would be quite interesting as it would result in a novel, spin-orbital entangled electron gas, with properties quite different from the 2DEG in the 3d oxide structures such as the well-studied LaAlO₃/SrTiO₃ interface.

This research was supported by the U.S. Department of Energy, Office of Basic Energy Sciences, Division of

-
- ¹ B. J. Kim, H. Jin, S. J. Moon, J.-Y. Kim, B.-G. Park, C. S. Leem, J. Yu, T. W. Noh, C. Kim, S.-J. Oh, J.H. Park, V. Durairaj, G. Cao, and E. Rotenberg, Novel $J_{\text{eff}} = 1/2$ Mott State Induced by Relativistic Spin-Orbit Coupling in Sr_2IrO_4 , *Phys. Rev. Lett.* **101**, 076402 (2008).
 - ² K. Yang Yu., Y. M. Lu, and Y. Ran, Quantum Hall effects in a Weyl semimetal: Possible application in pyrochlore iridates, *Phys. Rev. B* **84**, 075129 (2011).
 - ³ W. W. Krempa, G. Chen, Y. B. Kim, and L. Balents, Correlated Quantum Phenomena in the Strong Spin-Orbit Regime, *Ann. Rev. Cond. Matt. Phys.* **5**, 57 (2014).
 - ⁴ X. Wan, A. Vishwanath, and S. Y. Savrasov, Computational Design of Axion Insulators Based on 5d Spinel Compounds, *Phys. Rev. Lett.* **108**, 146601 (2012).
 - ⁵ L. Balents, Spin liquids in frustrated magnets, *Nature* **464**, 199 (2010).
 - ⁶ M. J. Lawler, A. Paramakanti, Y. B. Kim, and L. Balents, Gapless Spin Liquids on the Three-Dimensional Hyperkagome Lattice of $\text{Na}_4\text{Ir}_3\text{O}_8$, *Phys. Rev. Lett.* **101**, 197202 (2008).
 - ⁷ C. Bhandari and S. Satpathy, Spin-orbital entangled two-dimensional electron gas at the $\text{LaAlO}_3/\text{Sr}_2\text{IrO}_4$ interface, *Phys. Rev. B* **98**, 041303(R) (2018) (<https://doi.org/10.1103/PhysRevB.98.041303>).
 - ⁸ Z. S. Popović, S. Satpathy, and R. M. Martin, Origin of the Two-Dimensional Electron Gas Carrier Density at the LaAlO_3 on SrTiO_3 Interface, *Phys. Rev. Lett.* **101**, 256801 (2008).
 - ⁹ J. Matsuno, K. Ihara, S. Yamamura, H. Wadati, K. Ishii, V. V. Shankar, K. H-Y Kee, and H. Takagi, Engineering a Spin-Orbital Magnetic Insulator by Tailoring Superlattices, *Phys. Rev. Lett.* **114**, 247209 (2015).
 - ¹⁰ L. M. Ying, L. Z. Tai, Y. H. Feng, Z. J. Lin, Y. Qi, F. C. Cong, J. S. Liu, G. Bo, S. Da-Wei, and X. Xiao-Ming, Tuning the Electronic Structure of Sr_2IrO_4 Thin Films by Bulk Electronic Doping Using Molecular Beam Epitaxy, *Chinese Physics Letters*, **32**, (2015).
 - ¹¹ D. J. Groenendijk, N. Manca, G. Mattoni, L. Kootstra, S. Gariglio, Y. Huang, E. van Heumen, and A. D. Caviglia, Epitaxial growth and thermodynamic stability of $\text{SrIrO}_3/\text{SrTiO}_3$ heterostructures, *Appl. Phys. Lett.* **109**, 041906 (2016).
 - ¹² T. F. Qi, O. B. Korneta, L. Li, K. Butrouna, V. S. Cao, X. Wan, P. Schlottmann, R. K. Kaul, and G. Cao, Spin-orbit tuned metal-insulator transitions in single-crystal $\text{Sr}_2\text{Ir}_{1-x}\text{Rh}_x\text{O}_4$ ($0 \leq x \leq 1$), *Phys. Rev. B* **86**, 125105 (2012).
 - ¹³ J. Nichols, J. Terzic, E. G. Bittle, O. B. Korneta, L. E. De Long, J. W. Brill, G. Cao, and S. S. A. Seo, Tuning electronic structures via epitaxial strain in Sr_2IrO_4 thin films, *Appl. Phys. Lett.* **102**, 141908 (2013).
 - ¹⁴ C. R. Serrao, J. Liu, J. T. Heron, G. Singh-Bhalla, A. Yadav, S. J. Suresha, R. J. Paull, D. Yi, J.-H. Chu, M. Trassin, A. Vishwanath, E. Arenholz, C. Frontera, J. Zelezny, T. Jungwirth, X. Marti, and R. Ramesh, *Phys. Rev. B* **87**, 085121 (2013).
 - ¹⁵ L. D. Miao, H. Xu, and Z. Q. Mao, Epitaxial strain effect on the $J_{\text{eff}} = 1/2$ moment orientation in Sr_2IrO_4 thin films *Phys. Rev. B* **89**, 035109 (2014).
 - ¹⁶ J. S. Lee, Y. Krockenberger, K. S. Takahashi, M. Kawasaki, and Y. Tokura, Insulator-metal transition driven by change of doping and spin-orbit interaction in Sr_2IrO_4 , *Phys. Rev. B* **85**, 035101 (2012).
 - ¹⁷ Y. K. Kim, O. Krupin, J. D. Denlinger, A. Bostwick, E. Rotenberg, Q. Zhao, J. F. Mitchell, J. W. Allen, and B. J. Kim, Superconductivity. Fermi arcs in a doped pseudospin-1/2 Heisenberg antiferromagnet, *Science* **345**, 6193 (2014).
 - ¹⁸ M. Ge, T. F. Qi, O. B. Korneta, D. E. De Long, P. Schlottmann, W. P. Crummett, and G. Cao, Lattice-driven magnetoresistivity and metal-insulator transition in single-layered iridates, *Phys. Rev. B* **84**, 100402 (2011).
 - ¹⁹ O. B. Korneta, T. F. Qi, S. Chikara, S. Parkin, L. E. De Long, P. Schlottmann, and G. Cao, Electron-doped $\text{Sr}_2\text{IrO}_{4-\delta}$ ($0 \leq \delta \leq 0.04$): Evolution of a disordered $J_{\text{eff}}=12$ Mott insulator into an exotic metallic state, *Phys. Rev. B* **82**, 115117 (2010).
 - ²⁰ H. Gretarsson, N. H. Sung, J. Porras, J. Bertinshaw, C. Dietl, J. A. N. Bruin, A. F. Bangura, Y. K. Kim, R. Dinnebier, J. Kim, A. Al-Zein, M. Moretti Sala, M. Krisch, M. Le Tacon, B. Keimer and B. J. Kim, Persistent Paramagnons Deep in the Metallic Phase of $\text{Sr}_{2-x}\text{La}_x\text{IrO}_4$, *Phys. Rev. Lett.* **117**, 107001 (2016).
 - ²¹ X. Chen, T. Hogan, D. Walkup, W. Zhou, M. Pokharel, M. Yao, W. Tian, T. Z. Ward, Y. Zhao, D. Parshall, C. Opeil, J. W. Lynn, V. Madhavan, and S. D. Wilson, Influence of electron doping on the ground state of $(\text{Sr}_{1-x}\text{La}_x)_2\text{IrO}_4$, *Phys. Rev. B* **92**, 075125 (2015).
 - ²² A. de la Torre, S. M. Walker, F. Y. Bruno, S. Riccò, Z. Wang, I. L. Gutierrez, G. Scheerer, G. Girit, D. Jaccard, C. Berthod, T. K. Kim, M. Hoesch, E.C. Hunter, R.S. Perry, A. Tamai, and F. Baumberger, Collapse of the Mott Gap and Emergence of a Nodal Liquid in Lightly Doped Sr_2IrO_4 , *Phys. Rev. Lett.* **115**, 176402 (2015).
 - ²³ Z. S. Popović and S. Satpathy, Wedge-Shaped Potential and Airy-Function Electron Localization in Oxide Superlattices, *Phys. Rev. Lett.* **94**, 176805 (2005).
 - ²⁴ Y. Matsubara, K. S. Takahashi, M. S. Bahramy, Y. Kozuka, D. Maryenko, J. Falson, A. Tsukazaki, Y. Tokura, and M. Kawasaki, Observation of the quantum Hall effect in δ -doped SrTiO_3 , *Nat. Commun.* **7**, 11631 (2016).
 - ²⁵ For details of the methods, see: <https://www.questaal.org>.
 - ²⁶ M. Methfessel, M. van Schilfgaarde, and R.A. Casali, A Full-Potential LMTO Method Based on Smooth Hankel Functions, Electronic Structure and Physical Properties of Solids. The Use of the LMTO Method, *Lecture Notes in Physics* **535**, 114 (2000).
 - ²⁷ K. Takao and M. van Schilfgaarde, Fusion of the LAPW and LMTO methods: The augmented plane wave plus muffin-tin

- orbital method, Phys. Rev. B **81**, 125117 (2010).
- ²⁸ U. von Barth and L. Hedin, A local exchange-correlation potential for the spin polarized case. i, Journal of Physics C: Solid State Physics **5**, 1629 (1972).
- ²⁹ W. Kohn and L. J. Sham, Self-Consistent Equations Including Exchange and Correlation Effects, Phys. Rev. **140**, A1133 (1965).
- ³⁰ G. Kresse and J. Hafner, Ab initio molecular dynamics for liquid metals Phys. Rev. B **47**, 558(R) (1993).
- ³¹ P. E. Blöchl, Projector augmented-wave method, Phys. Rev. B **50**, 17953 (1994).
- ³² S. L. Dubarev, G. A. Botton, S. Y. Savrasov, C. J. Humphreys, and A. P. Sutton, Electron-energy-loss spectra and the structural stability of nickel oxide: An LSDA+U study, Phys. Rev. B **57**, 1505 (1998).
- ³³ C. Bhandari, Z. S. Popović, and S. Satpathy, Electronic structure and optical properties of Sr₂IrO₄ under epitaxial strain, New J. Phys. **21**, 013036 (2019) (<https://doi.org/10.1088/1367-2630/aaff1b>).
- ³⁴ G. Cao, J. Bolivar, S. McCall, J. E. Crow, and R. P. Guertin, Weak ferromagnetism, metal-to-nonmetal transition, and negative differential resistivity in single-crystal Sr₂IrO₄, Phys. Rev. B **57**, 11039(R) (1998).